JOC The Journal of Organic Chemistry

Article

pubs.acs.org/joc

Design and Synthesis of Photodissociable Ligands Based on Azoimidazoles for Light-Driven Coordination-Induced Spin State Switching in Homogeneous Solution

Christian Schütt, Gernot Heitmann, Thore Wendler, Bahne Krahwinkel, and Rainer Herges*

Otto Diels-Institute for Organic Chemistry, University of Kiel, Otto-Hahn-Platz 4, Kiel D-24119, Germany

Supporting Information

ABSTRACT: Light-switchable azoimidazoles were rationally designed and synthesized, and their performance was investigated as photodissociable ligands (PDL) and for spin state switching of Ni porphyrins. The rationally designed ligands exhibit a high photochemical conversion rate (*trans* → *cis* > 98%) and no measurable fatigue over a large number of switching cycles at room temperature under air. As compared to the known phenylazopyridines, the phenylazoimidazoles exhibit a much stronger affinity as axial ligands to Ni porphyrin in the binding *trans* configuration and a low affinity in their *cis* form. This affinity switching was used to control the coordination number of Ni^{2+}. Concomitant with the change in coordination number is the change of the spin state from triplet (high spin) to singlet state (low spin). We report on phenylazoimidazole-based PDLs that switch the paramagnetic ratio of the investigated nickel species by up to 70%. Consequently, azoimidazoles exhibit considerably higher switching efficiencies than previously described pyridine-based PDLs.

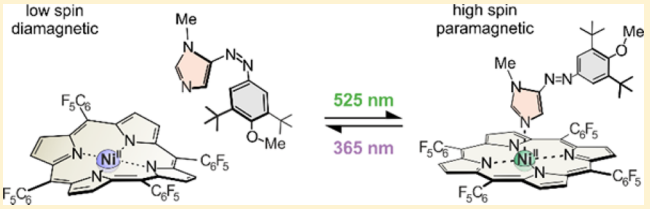

INTRODUCTION

Switchable ligands for photocontrolled binding are of general interest in a large number of fields. Practical applications range from the reversible switching of the activity of drugs, inhibitors, ion channels, and chemical optogenetics.[1−3] Particularly important as well is the light control of optical, electric, and magnetic properties of materials (such as the orientation of the magnetization or the magnetic susceptibility). Magnetic bistability at room temperature is a typical materials property. Cooperative effects between a large number of spin centers in the solid state stabilize the magnetic states and lead to hysteresis.[4] Notably, spin crossover and the light-induced excited spin state trapping (LIESST) phenomenon have been used to switch the spin state in crystals of transition metal complexes.[5] Until recently, however, there was little work on spin switching in the solution phase[6,7] or on single molecules at surfaces,[8,9] even though this would open a number of interesting applications, such as data storage or their use as switchable contrast agents in MRI. For achieving bistability in isolated molecules, the solid state cooperative effects have to be replaced by molecule inherent mechanisms. We have recently demonstrated that the spin state of isolated molecules can be switched between low spin (diamagnetic) and high spin (paramagnetic) using light.[10−13] Our approach is based on the fact that a number of transition metal ions (e.g., Fe^{2+}, Fe^{3+}, Co^{2+}, Ni^{2+}) change the spin state upon changing their coordination number. We chose Ni^{2+} because it is stable in its oxidation state and the spin state change is reliable and predictable. Square planar (4-coordinate) Ni^{2+} is low spin (S = 0), and square pyramidal (5-coordinate) or square bipyramidal (6-coordinate) Ni^{2+} are high spin (S = 1).[14−19] Coordination change, and thus spin change, is achieved by adding and removing axial ligands from a square planar Ni porphyrin (Figure 1).[20]

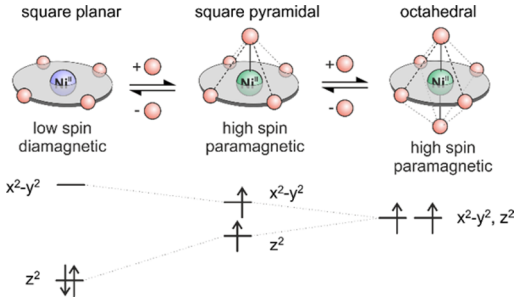

Figure 1. Coordination-induced spin state switch (CISSS) in Ni(II) complexes.

Light-induced axial ligand association and dissociation is operated either by tethering the switchable ligands to the square planar Ni porphyrin (record player design)[11,13,21] or by properly designed photodissociable ligands (PDLs).[10,12] Both designs have pros and cons. "Record player" complexes that move the coordinating nitrogen up and down like a tone arm the needle exhibit a large switching efficiency; however, at large concentrations, they undergo intermolecular coordination. PDLs, if properly designed, are sterically hindered in one of the two photoisomers, which prevents inter- as well as intramolecular coordination. Moreover, new types of PDLs

Received: December 11, 2015
Published: January 13, 2016

DOI: 10.1021/acs.joc.5b02817
J. Org. Chem. 2016, 81, 1206−1215

might also find applications as switchable drugs, inhibitors, or other biochemical probes. The most frequently used PDLs are probably azopyridines.[22−25] They combine the photochromism of azobenzene and the coordination properties of pyridine in one small molecule and are easy to synthesize. Other heterocyclic azo compounds are scarce.[26] Azo heterocycles with a higher basicity, nucleophilicity, and coordination power than azopyridines would be particularly valuable for the switching of functions, such as spin state switching, or the control of binding properties, e.g., in active sites of enzymes. We chose imidazole as the heterocycle, replacing one phenyl group in azobenzene. The binding constant of *N*-methylimidiazole to Ni porphyrins is more than an order of magnitude higher compared to pyridine and three times the value of 4-methoxypyridine.[27] There are three regioisomers of phenyl azoimidazoles (azo group in 2, 4, and 5 position if tautomerism is prevented by substitution at N-1). However, imidazoles that bear substituents adjacent to the coordinating nitrogen (in 2- and 4-position) do not coordinate to metal porphyrins for steric reasons (Figure 2).[28,29] Only 5-phenylazoimidazoles are potential candidates for coordination switching (see also coordination of histidine to iron in hemoglobin as an example in nature).

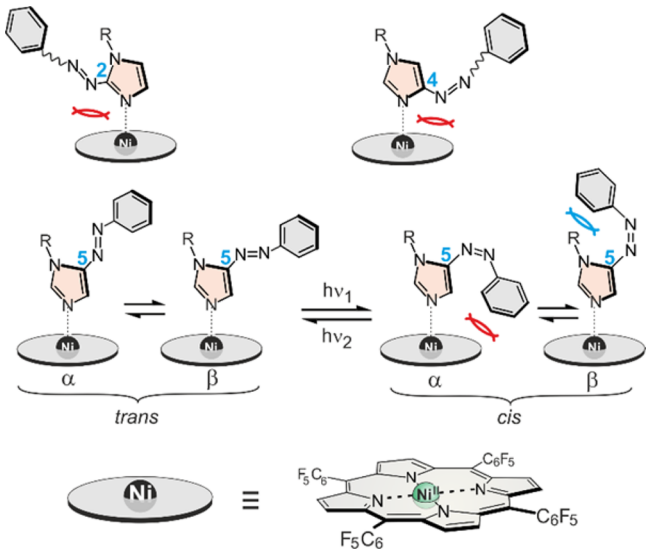

Figure 2. Schematic representation of the steric implications upon coordination of different phenylazoimidazoles to metal porphyrins. Imidazoles with substituents next to the coordinating nitrogen (2- and 4-phenylazoimidazole) do not bind to the metal for steric reasons (red arcs). Only 5-phenylazoimidazole provides a basis for the development of PDLs. The *trans* and the *cis* isomers each can adopt two conformations (α and β). Both *trans* conformations are binding. One of the *cis* conformations (α) exhibits sterical problems upon coordination (red arcs); however, the β conformation does not. The *cis*-β conformer would still bind, and photoisomerization of the ligand would not lead to photodissociation. However, formation of the *cis*-β conformation could be hampered by steric interaction of the substituent R at N-1 and the phenyl ring (blue arcs).

We recently published a convenient synthesis for the hitherto unknown 5-phenylazoimidazoles using a novel type of azocoupling of lithiated imidazole with benzene diazonium salts.[30] We now report on the rational design of substituted 5-phenylazoimidazoles, which are structurally optimized with respect to their switching efficiency (SE). The switching efficiency is defined as the difference of a target parameter in the two switching states. In a two-component system (metal complex/photodissociable ligand or receptor/photoswitchable inhibitor), it seems obvious that the maximum switching efficiency (SE_{max}) depends on the concentration of both components. Surprisingly, this is not the case. There is an optimal ligand concentration ($[L]_{opt}$) that leads to the maximum switching efficiency (SE_{max}) independent of the metal complex (receptor) concentration.[12] The maximum switching efficiency and the optimal ligand concentration are system parameters. The most important conclusion that we draw from this finding is that it is more important to optimize the conversion to the non-binding isomer and to reduce its coordination by steric hindrance than optimizing the binding state.

RESULTS AND DISCUSSION

Steric Design at the Imidazole. The starting point of our design was the introduction of bulky substituents in such a way that the binding of the *cis* isomer would be impaired while leaving the coordination of the *trans* form unaffected. To achieve this goal, one has to consider that both isomers have two conformations. To prevent the *cis* isomer from binding, both conformations (*cis*-α and *cis*-β, Figure 2) have to be included in the design process. In contrast to the *cis*-α conformer, the coordination of the *cis*-β conformer to the porphyrin is not sterically hindered because the phenyl group points away from the porphyrin (Figure 2, right). Thus, it is obvious that steric constraints have to be introduced at the N-1 position (Figure 2, right, blue arcs) to disfavor the formation of the *cis*-β conformation. For predicting which substituent would be needed to sufficiently disfavor the *cis*-β conformer, quantum chemical calculations were performed using the program TURBOMOLE[31] 6.3 at the PBE/SVP level of DFT. The relative energies show that in the parent system (R^1 = H, **1**) both conformations *cis*-α and *cis*-β are almost equal in energy (Figure 3). Upon introducing a methyl group (R^1 = Me, **2**) in the 1-position of the imidazole, the formation of the *cis*-β conformer is already disfavored by more than 5 kcal mol^{-1}.

Further increasing the steric repulsion between the 1-position and the phenyl ring leads to a larger energy difference of the two

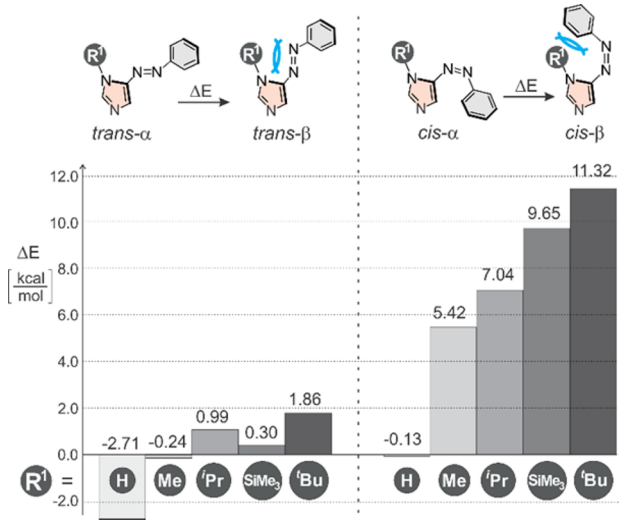

Figure 3. Bar diagram of the energy difference ($E_\beta - E_\alpha$) of the α and β conformation of several N-1-substituted azoimidazoles at the PBE/SVP level of theory. Energies are given in kcal mol^{-1}. Intramolecular steric repulsion is indicated by blue arcs.

DOI: 10.1021/acs.joc.5b02817
J. Org. Chem. 2016, 81, 1206−1215

cis conformers. The introduction of an isopropyl group in the 1-position (**3**, ΔE = 7.04 kcal mol^{-1}) disfavors the formation of the *cis*-β conformer roughly by an additional 1.5 kcal mol^{-1}, whereas substitution with a trimethylsilyl- (**4**, ΔE = 9.65 kcal mol^{-1}) or *tert*-butyl-group (**5**, ΔE = 11.32 kcal mol^{-1}) leads to a significantly larger energy difference compared to phenylazoimidazole **2** (see Figure 3). As a result, the non-binding *cis*-α conformer should be the predominant species in solution in all cases except R = H. To gain information on how substitution (R^1) at N-1 would affect the coordination of the *trans* and the *cis* ligands to Ni porphyrins, and more specifically, if disfavoring the binding *cis*-β conformation would be sufficient to obtain an efficient photodissociable ligand, we calculated the binding energy of the four species (*trans*-α, *trans*-β, *cis*-α, and *cis*-β) of azoimidazoles **1**−**5** to the Ni porphyrin $NiTPPF_{20}$ at the B3LYP/def2TZVP//PBE/SVP level of density functional theory. This level has proven to yield reliable results for the formation of complexes of 1-methylimidazole (see Supporting Information) with $NiTPPF_{20}$ (Table 1). Because the α and β conformations are

Table 1. Calculated Complex Formation Energies (ΔE_f, kcal mol^{-1}) of 1−5 (see Figure 4) with $NiTPPF_{20}$ at the B3LYP/def2TZVP//PBE/SVP Level of Theory

	R^1	*trans*-α	*trans*-β	*cis*-α	*cis*-β	$\Delta\Delta E_{f,calc}$ [a]
1	H	−4.35	−7.70	−5.18	−6.67	1.03
2	Me	−7.70	−8.08	−5.20	−0.65	2.88
3	^{i}Pr	−8.54	−7.07	−6.66	−0.79	1.88
4	$SiMe_3$	−7.42	−6.79	−6.86	3.63	0.57
5	^{t}Bu	−8.24	−4.26	−6.44	3.44	1.80

[a]Energy difference of ΔE_f of the strongest binding *trans* and *cis* conformer.

in fast equilibrium, the complex formation energies listed in Table 1 are relative to the most stable conformation. The calculated binding energies in Table 1 and Figure 4 clearly predict that the parent system (R = H) would bind strongly in all configurations and conformations, and therefore, it would be a very inefficient photodissociable ligand. Introduction of a methyl group at N-1, as expected, prevents the formation of the complex of the *cis*-β species with $NiTPPF_{20}$ almost completely (ΔE_f = −0.65 kcal mol^{-1}). For the larger substituents $SiMe_3$ and ^{t}Bu, complex formation of the *cis*-β species is predicted to be endothermic (3.63 and 3.44 kcal mol^{-1}).

Even though introduction of substituents such as Me, ^{i}Pr, $SiMe_3$, and ^{t}Bu at the imidazole nitrogen efficiently prevent the formation of the complexes with the β-*cis* ligand, the α-*cis* ligands still bind with ΔE_f < −5 kcal mol^{-1}. Obviously, steric interaction of the phenyl group with the porphyrin (red arcs in Figure 4) is not sufficient to disfavor complex formation. Therefore, the steric hindrance of the phenyl group has to be increased by substitution of the phenyl ring with bulky substituents.

Photophysical Design of the Ligand. The photophysical properties of the parent azoimidazole switch, 1-methyl-5-phenylazoimidazole (**2**), have been recently investigated.[30] The light-induced conversion (365 nm) of the more stable *trans* to *cis* state is extremely efficient (>99%), and the thermal back reaction is very slow ($t_{1/2}$ = 22 days at 25 °C). Unfortunately, the light-induced isomerization of the *cis* isomer back to the *trans* form with visible light (455 nm) is incomplete (40%) because there is a considerable overlap of the π−π* and n−π* bands in the *cis* configuration. To improve the photochemical back reaction, we synthesized several derivatives of 1-methyl-5-phenyl azoimidazole (**2a**−**c**, Figure 5). Electron-donating and -withdrawing groups were introduced at the phenyl group. Substitution with

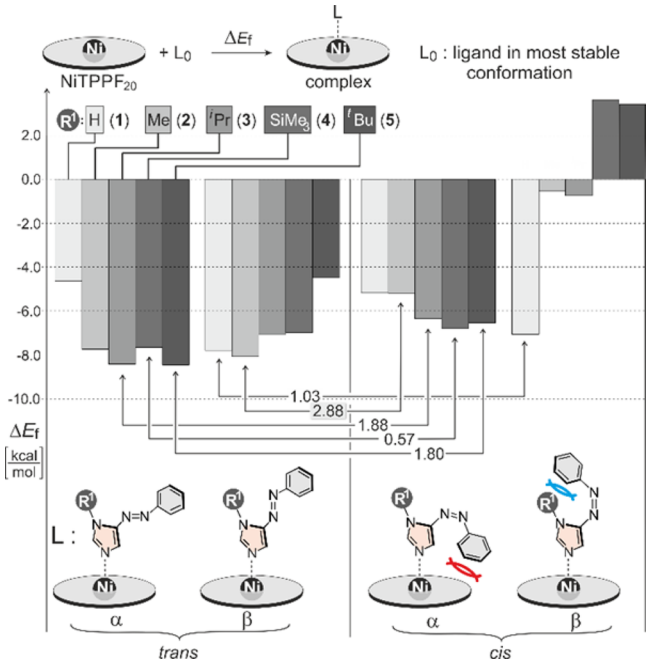

Figure 4. Calculated (B3LYP/def2TZVP//PBE/SVP) complex formation energies (ΔE_f in kcal mol^{-1}) of phenylazoimidazole derivatives (**1**−**5**) with $NiTPPF_{20}$. The definition of the complexation energy (ΔE_f) is given on top. Intermolecular and intramolecular steric hindrance is indicated with red and blue arcs. The energy differences between the strongest binding *trans* and *cis* conformations of each ligand are indicated by arrows. The *N*-methyl-substituted ligand (**2**) exhibits the largest change in binding energy ($\Delta\Delta E_f$ = 2.88 kcal mol^{-1}) upon *trans*-*cis* isomerization.

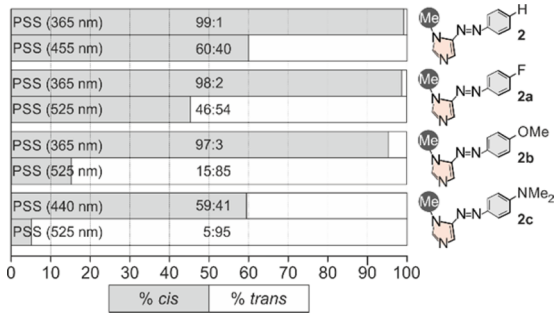

Figure 5. Photostationary states of 4′-substituted 1-methyl-5-phenylazoimidazoles determined by UV spectroscopy. Irradiation times: 20 min.

fluorine in the *para* position (**2a**) improves the photostationary state (PSS) at 525 nm from 40 to 54% *trans*, whereas the *trans* to *cis* isomerization (PSS 365 nm) is almost unchanged. The introduction of electron-donating groups in the *para* position further improves the *cis* to *trans* conversion (PSS 525 nm) with increasing donor strength from 85% (OMe, **2b**) to 95% (NMe_2, **2c**). However, although the *trans* to *cis* conversion is almost unchanged for **2b** (97%), the photo-induced switching to the *cis* isomer in **2c** decreases to 59% (Figure 5). TD-DFT calculations (see Supporting Information) provide a rational understanding of the experimental results. They predict the largest separation of the π−π* and n−π* bands for **2b**.

DOI: 10.1021/acs.joc.5b02817
J. Org. Chem. 2016, 81, 1206−1215

The results of the experimental and theoretical investigations lead to the conclusion that a methoxy group in the *para* position of the phenyl ring is the most effective substituent to improve the switching efficiency of 5-phenyl-azoimidazoles. Therefore, **2b** is a promising starting point for the further design of PDLs.

Steric Design at the Phenyl Group. As stated before, the PDL design has to include both conformations (α and β) of the *cis* isomer. For preventing the *cis* isomer from binding, the formation of the β conformation was suppressed by introduction of a methyl group at the imidazole ring (Figure 3). However, as predicted by theoretical calculations, steric hindrance in the α conformation obviously is not sufficient to prevent the parent system **2** from binding (Table 1, Figure 4). Therefore, we have to increase the steric demand of the phenyl group by the introduction of bulky substituents (Figure 6).

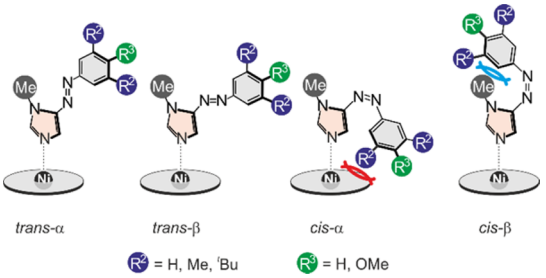

Figure 6. Binding modes of *trans*- and *cis*-1-methylphenylazoimidazole derivatives. Intermolecular steric hindrance of the *cis* isomer with $NiTPPF_{20}$ is indicated with red curved lines. Intramolecular hindrance is indicated by blue arcs.

We calculated the complex formation energies of the photophysically optimized methoxy derivative **2b** and the sterically more demanding systems **2d** and **2e** with $NiTPPF_{20}$ at the B3LYP/def2TZVP//PBE/SVP level of theory to quantify the effect of the steric bulk (Figure 7 and Table 2).

The calculations predict that two *t*-butyl groups in the *meta* position are most effective in preventing the α conformation from binding to the Ni porphyrin. Methyl substituents in the *meta* position or the methoxy group in the *para* position are considerably less effective.

Thus, **2e** is the most promising candidate for an effective PDL. The methoxy group in the *para* position improves the photophysical properties; the methyl group at the imidazole ring suppresses the formation of the β conformation, and the two *t*-butyl substituents prevent the α conformation from binding.

Synthesis and Properties of the Improved PDL. Azoimidazole **2e** was synthesized analogously to a previously published strategy.[30] The key step is the directed lithiation of a doubly protected imidazole and the reaction with a phenyldiazonium salt (prepared as tetrafluoroborate in five steps out of 3,5-di-*tert*-butyl-4-hydroxybenzoic acid; overall yield of 31%), forming the azo compound by a polar C−N bond formation (Scheme 1). Both protecting groups at the imidazole are then removed. A trityl (Tr) group is regioselectively introduced at the sterically less hindered nitrogen. Subsequent methylation of the second nitrogen leads to the imidazolium ion, which easily cleaves the Tr group leading to the desired 1,5 substitution pattern at the imidazole ring. The overall yield over nine steps (starting from sulfamoyl imidazole) is 37%. The preparation is quite convenient because only two intermediate compounds have to be isolated in the three pot reaction.

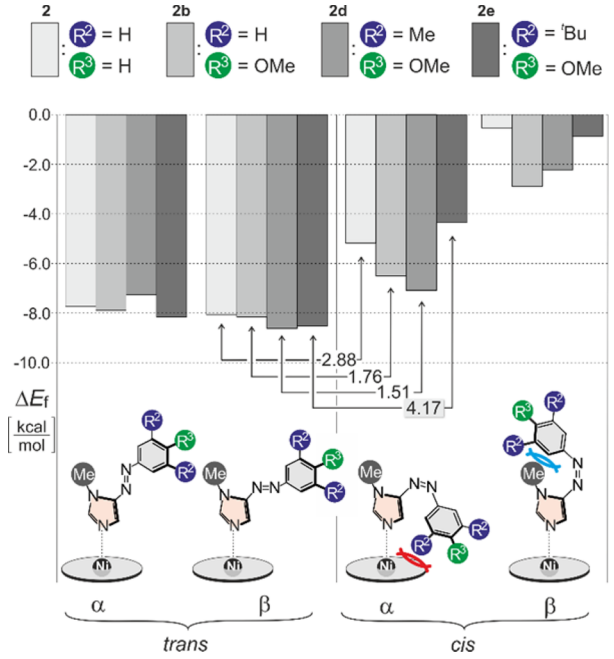

Figure 7. Calculated (B3LYP/def2TZVP//PBE/SVP) complex formation energies. The energy difference between the *trans*-β conformer and strongest binding *cis* configuration of the considered ligands are indicated by arrows. Ligand **2e** exhibits the largest change in binding energy ($\Delta\Delta E_f$ = 4.17 kcal mol^{-1}) upon *trans-cis* isomerization. Energies are given in kcal mol^{-1}. Intermolecular and intramolecular steric repulsion is indicated with red and blue arcs.

Table 2. Calculated Complex Formation Energies (ΔE_f, kcal mol^{-1}) of 2, 2b, 2d, and 2e (see Figure 7) with $NiTPPF_{20}$ (B3LYP/def2TZVP//PBE/SVP)

	trans-α	*trans*-β	*cis*-α	*cis*-β	$\Delta\Delta E_{f,calc}$ [a]
2	−7.70	−8.08	−5.20	−0.65	2.88
2b	−7.86	−8.16	−6.40	−2.98	1.76
2d	−7.15	−8.45	−6.94	−2.07	1.51
2e	−8.20	−8.43	−4.26	−0.79	4.17

[a]Energy difference of ΔE_f of the strongest binding *trans* and *cis* conformer.

We determined the association constants (K) and enthalpies of complex formation (ΔH) of the *cis* and *trans* isomer of **2e** with $NiTPPF_{20}$ using a previously developed NMR titration method (for details, see the Supporting Information).[10] For comparison with the theoretically predicted energies of complex formation and to quantify the improvement of the switching efficiency by our molecular design, we also included the parent system **2** and **2b** in our experimental studies. Table 3 summarizes the experimental values for K_{1S} and ΔH_{1S} (formation of the 1:1 complex) for **2**, **2b**, and **2c** in *cis* and *trans* configurations. Our molecular design strategy aims at increasing the difference in binding energy of the *cis* and *trans* isomer ($\Delta\Delta H_{1S}$). Introduction of the two *tert*-butyl substituents in **2e** indeed decreases the binding energy of the *cis* isomer substantially while having little effect on the association of the *trans* form. The ratio between the *trans* and *cis* association constants ($K_{1S,trans}/K_{1S,cis}$) in the parent system (**2**) is 3.60 and increases to 43.8 in the sterically hindered system **2e** (Table 3). It is noteworthy that the experimentally derived binding enthalpy differences are in good agreement with the calculated values (Table 3).

DOI: 10.1021/acs.joc.5b02817
J. Org. Chem. 2016, 81, 1206−1215

Scheme 1. Synthesis of Azoimidazole 2e[a]

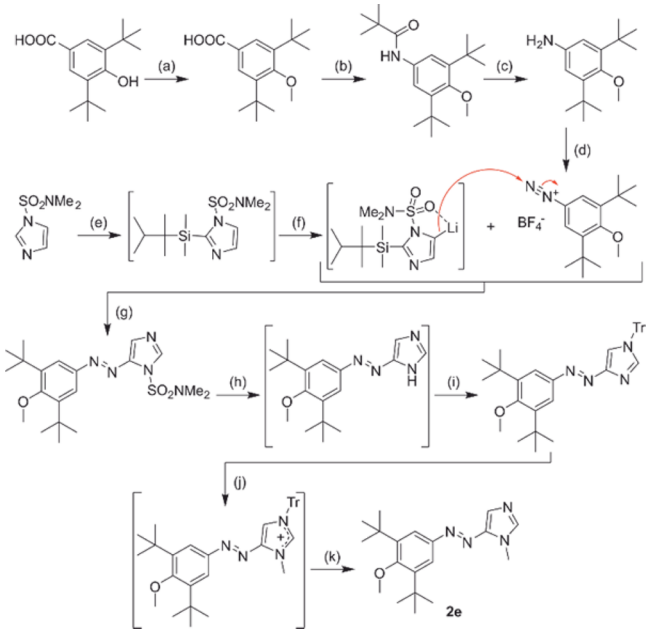

[a]Reagents and conditions. (a) 1. MeI, KOH, acetone, 60 °C, 18 h; 2. LiOH, THF, H_2O, 60 °C, 18 h, 71%; (b) DPPA, Et_3N, ^tBuOH, 85 °C, 18 h, 72%; (c) TFA, CH_2Cl_2, rt, overnight, 92%; (d) isopentyl nitrite, HBF_4 (aq), EtOH, rt, 15 min, 65%; (e) 1. *n*-BuLi, THF, −78 °C, 30 min; 2. dimethylthexylchlorosilane, THF, −78 °C to rt, overnight; (f) *n*-BuLi, THF, −78 °C, 30 min; (g) 1. THF, −78 °C to rt, overnight; 2. TBAF trihydrate, CsF, THF, rt, overnight, 58% (5 steps, 1 pot); (h) HCl, EtOH, 50 °C, 3 h; (i) trityl chloride, Et_3N, CH_2Cl_2, rt, overnight, 77% (2 steps, 1 pot); (j) 1. methyl triflate, CH_2Cl_2, rt, overnight; (k) H_2O, acetone, CH_2Cl_2, rt, 3 h, 82%.

Table 3. Experimentally Determined Association Constants (K_{1S}) and Binding Enthalpies (ΔH_{1S}) for Coordination of the *trans* and *cis* Isomers of 2, 2b, and 2e to $NiTPPF_{20}$

	2	2b	2e
$K_{1S,trans}$ [a]	38.31	59.14	60.03
$\Delta H_{1S,trans}$ [b]	−6.84	−6.63	−7.10
$K_{1S,cis}$ [a]	10.76	15.83	1.37
$\Delta H_{1S,cis}$ [b]	−4.69	−4.97	−3.01
$\Delta\Delta H_{1S}$ [c]	2.15	1.66	4.09
$\Delta\Delta E_{1S}$ [d]	2.88	1.75	4.18

[a]At 298 K for **2** and **2b**, 300 K for **2e**, toluene-d_8, [L mol^{-1}]. [b]In [kcal mol^{-1}]. [c]Experimental binding enthalpy differences to $NiTPPF_{20}$ ($\Delta\Delta H_{1S} = \Delta H_{1S,cis} - \Delta H_{1S,trans}$) [kcal mol^{-1}]. [d]Calculated binding energy differences (B3LYP/def2TZVP//PBE/SVP) to $NiTPPF_{20}$ ($\Delta\Delta E_{1S} = \Delta E_{1S,cis} - \Delta E_{1S,trans}$) [kcal mol^{-1}].

Switching Experiments. On the basis of the experimentally determined association constants (K_{1s}, K_2, for data, see the Supporting Information) of the *trans* and *cis* configurations of **2**, **2b**, and **2e**, the conditions for achieving the maximum switching efficiency SE_{max} can be theoretically calculated. The switching efficiency is defined as the difference of the properties of a system in the two switching states. The properties of interest are the amount of *cis* isomer, or in our case, even more interesting is the amount of paramagnetic species in solution in both photostationary states. A perfect system would exhibit 0% paramagnetic species in one switching state and 100% in the other state. SE_{max}, thus, would be 100%. Parameters that lower SE_{max} are incomplete photochemical conversions between *cis* and *trans*, incomplete binding of the *trans*, and residual binding of the *cis* isomer. Using a mathematical analysis, we have previously shown that there is an optimum ligand (PDL) concentration $[L]_{opt}$ that leads to a maximum switching efficiency (SE_{max}).[10] A plot of the switching efficiency as a function of the ligand (PDL) concentration of **2e** is given in Figure 8.

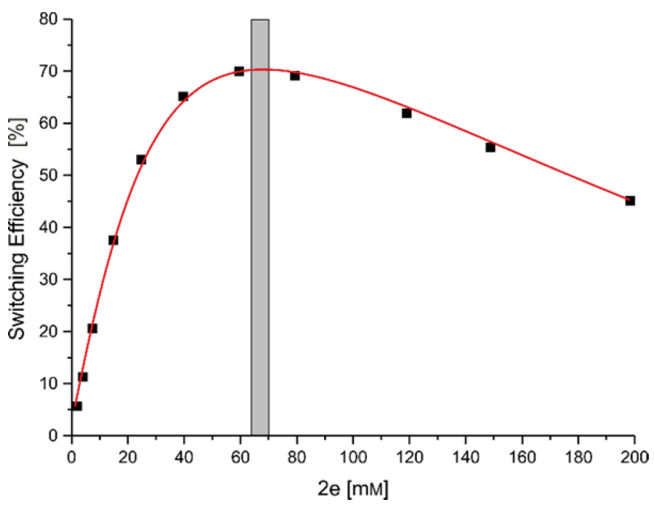

Figure 8. Switching efficiency (SE) (black squares) as a function of the ligand concentration of **2e** calculated from the experimentally determined association constants.[10] The maximum switching efficiency (SE_{max} = 70%) is predicted at a ligand concentration ($[L]_{opt}$) of 64.3 mM. The gray bar indicates the concentration used in our experiments (67.9 mM), which is close to the optimum ligand concentration.

The maximum switching efficiency SE_{max} for the system $NiTPPF_{20}$/**2e** is obtained at the optimum ligand concentration of **2e** ($[L]_{opt}$ = 64.3 mM). The optimum ligand concentrations for **2** and **2b** are 35.1 and 21.9 mM. Surprisingly, a rigorous mathematical treatment proves that $[L]_{opt}$ is independent of the receptor ($NiTPPF_{20}$) concentration over a concentration range from 0 to 4 mM. (Figure 9).

The switching experiments including **2**, **2b**, and **2e** were performed with concentrations close to the optimum ligand

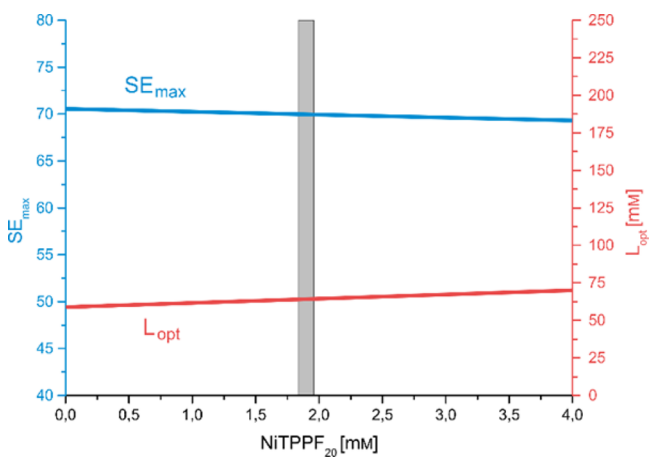

Figure 9. Maximum switching efficiency (SE_{max}) and optimal ligand concentration ($[L]_{opt}$) of **2e** as a function of the concentration of $NiTPPF_{20}$ (concentration range: 0−4 mM). In this region, SE_{max} and L_{opt} are independent from the concentration of $NiTPPF_{20}$. The gray bar indicates the concentration of **2e** used in our experiments (67.9 mM).

DOI: 10.1021/acs.joc.5b02817
J. Org. Chem. 2016, 81, 1206−1215

Table 4. Important Photochemical and Magnetic Switching Properties of Three Azoimidazoles (2, 2b, and 2e) and the to Date Most Efficient Azopyridine PDL 6[10] at Photostationary States PSS-365 and PSS-vis

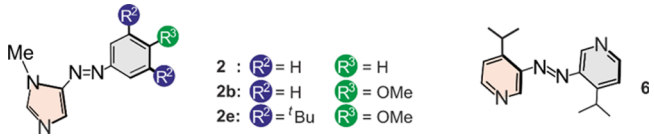

	% *cis* isomer[a]								% para. Ni^{2+}[f]		
	PSS-365	PSS-vis	$t_{1/2}$[b] [h]	$K_{1S\text{-}trans}$[c] [L mol^{-1}]	$K_{1S\text{-}cis}$[c] [L mol^{-1}]	$[L]_{opt}$[d] [mM]	SE_{max}[d] [%]	$[L]_{exptl}$[e] [mM]	$PSS_{365\ nm}$	PSS_{vis}	SE_{exptl}[f] [%]
2	98	67[g]	528	38.3	10.8	35.1	16	34.9	43	64	21
2b	95	22[h]	37.5	59.1	15.8	21.9	26	19.4	36	66	30
2e	98	49[h]	158	60.0	1.37	64.9	70	67.9	19	89	70
6	82	10[g]	262	9.99	0.30	91.9	50	69.2	21	68	48

[a]Amount of *cis* isomer in both photostationary states (PSS-365 and PSS-vis), 298 K, toluene-d_8, in the presence of $NiTPPF_{20}$ (1.94 mM for **2**, **2b**, and **2e**, 0.106 mM for **6**). [b]Thermal half-life of *cis* isomer, 298 K, toluene-d_8. [c]Association constants (K_{1S}) for *cis* and *trans* isomers determined from ^{1}H NMR titration experiments (for a full list of association constants, see the Supporting Information), 298 K for **2**, **2b**, and **6**, 300 K for **2e**, toluene-d_8, $NiTPPF_{20}$ (1.94 mM for **2**, **2b**, and **2e**, 0.106 mM for **6**). [d]Theoretically calculated optimal ligand concentrations ($[L]_{opt}$) and maximum switching efficiencies (SE_{max}) on the basis of experimentally determined association constants. [e]Ligand concentration used in the switching experiment. [f]Ratios of paramagnetic Ni^{2+} (% para. Ni^{2+}) in both photostationary states; the experimental switching efficiencies (SE_{exptl}) are determined on the basis of the porphyrin pyrrole shifts. [g]Irradiation with 455 nm. [h]Irradiation with 525 nm. Irradiation times were 20 min.

concentrations ($[L]_{opt}$). The experimental maximum switching efficiencies (SE_{exptl}) under these conditions are in good agreement with the theoretically predicted values (SE_{max}), supporting our mathematical model. Table 4 summarizes important properties of **2**, **2b**, and **2e**, including the parameters of azopyridine **6**, which has been the most efficient system so far.[10] Figure 10 shows a comparison of **6** with compound **2e**. The light-induced switching process is fully reversible without any sign of fatigue for both ligands over a large number of cycles.

To gain further insight into the compositions and concentrations of the complexes that are actually present in the solutions, we calculated the concentrations of the five possible complex species as a function of the ligand concentration (speciation plots, Figure 11). At the experimentally used ligand concentration ($[\mathbf{2e}] = [L]_{exptl} \cong [L]_{opt}$), the prevalent complex at PSS-365 is the bare $NiTPPF_{20}$ (81%, Figure 11a), and at PSS-525, the predominant species is the six-coordinate complex of $NiTPPF_{20}$ with two axial *trans*-**2e** ligands (55%, Figure 11b).

CONCLUSIONS

We present the most efficient photodissociable ligand (PDL) to date for light-driven, coordination-induced spin state switching (LD-CISSS). The coordination properties of imidazole were combined with the photochromic properties of azo compounds in a 5-phenylazoimidazole. The starting point of our design was the already published parent system,[30] which however exhibits an unsatisfying switching efficiency. We extensively used quantum chemical calculations to improve the properties by suitable substitution. The most promising candidates were synthesized and investigated. Azoimidazole **2e** turned out to be superior to previously used azopyridines (e.g., **6**)[10,12] in most aspects. The coordination power of the binding isomer is substantially higher, and smaller concentrations of the ligand are necessary for optimal switching. The photochemical conversion to the non-binding *cis* form is almost quantitative (98% as compared to 82% in azopyridine). Consequently, the switching efficiency was improved to 70% (as compared to 48% in azopyridine). Azoimidazoles are promising candidates to expand the coordination-induced spin state switching concept to other transition metal ions, such as Fe(II), Fe(III), and Mn(III). They are also suitable to be covalently tethered to the porphyrin core, a

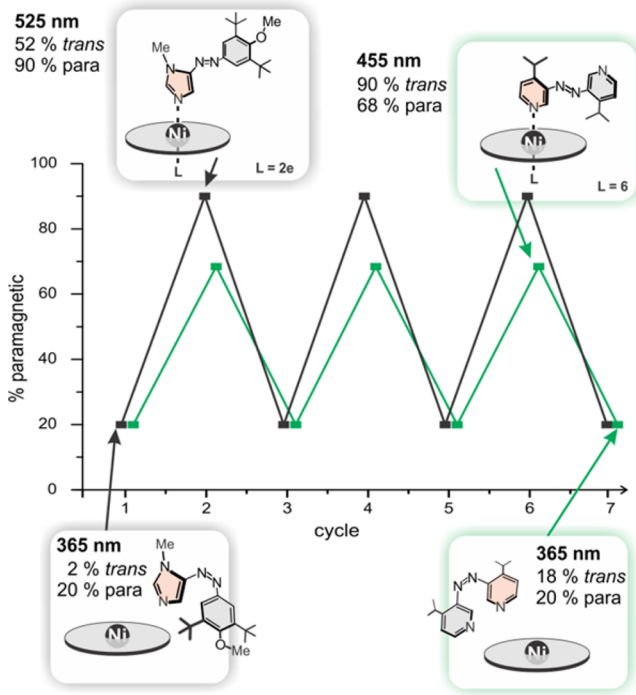

Figure 10. Reversible spin state switching of $NiTPPF_{20}$ with the PDL **2e** (azoimidazole, black curve) and **6**[10] (azopyridine, green curve). The proportion of paramagnetic nickel species is plotted as a function of the switching cycles. Switching was performed by irradiation with 365 nm (*trans* → *cis*) and 525 nm (**2e**) or 455 nm (**6**) (*cis* → *trans*). The azoimidazole ($[\mathbf{2e}] = 67.9$ mM, $[NiTPPF_{20}] = 1.94$ mM, toluene-d_8) exhibits a switching efficiency (SE) of 70%, whereas the azopyridine ($[\mathbf{6}] = 69.2$ mM, $[NiTPPF_{20}] = 0.106$ mM, toluene-d_8) is less efficient with SE = 48%. The predominant species at both PSSs are shown as simplified structures.

strategy that has been successfully used with azopyridines.[11,13] This so-called "record player" design has already been used to switch MRI contrasts.[21] Contrast agents based on the CISSS concept have a high potential for functional imaging in MRI and interventional radiology (minimal invasive, catheter-based

DOI: 10.1021/acs.joc.5b02817
J. Org. Chem. 2016, 81, 1206−1215

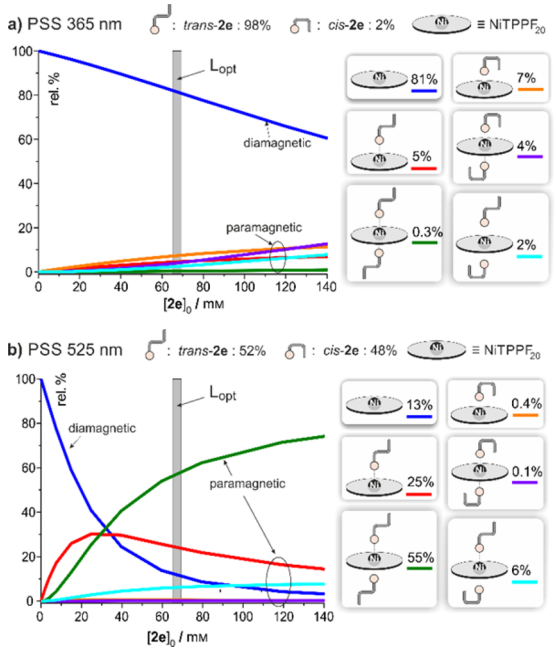

Figure 11. (a) Speciation plot of the six species in a solution of $NiTPPF_{20}$ (1.94 mM) in the presence of the *cis*/*trans* mixture of the ligand **2e** at PSS-365 (98% *cis*, 2% *trans*) and (b) speciation plot of the same solution at PSS-525 (48% *cis*, 52% *trans*). Both are given as a function of the total concentration of **2e** ($[\mathbf{2e}]_0 = [\textit{trans}\text{-}\mathbf{2e}] + [\textit{cis}\text{-}\mathbf{2e}]$). The proportion of the five complexes and free porphyrin at the ligand concentration used in the experiment $[\mathbf{2e}]_0 = [L]_{exptl} = 67.9$ mM, are given on the right. Note that only the free porphyrin is diamagnetic. All other complexes are paramagnetic.

surgery).[32−34] Azoimidazoles could improve and expand applications toward this end.

EXPERIMENTAL SECTION

General Experimental Methods. THF was dried and distilled from sodium/benzophenone. Dichloromethane was dried and distilled from CaH_2. *N,N*-Dimethylsulfamoylimidazole was synthesized analogously to the procedure of Chadwick et al.[35]

General Synthetic Procedure A. Synthesis of benzenediazonium tetrafluoroborates. If not stated otherwise, diazonium salts were prepared analogously to the procedure of Dunker et al.[36] Aniline (10.0 mmol) was suspended in tetrafluoroboric acid (20.0 mL, 50 wt % in water), and water was added until a clear solution was obtained. It was cooled to 0 °C, and sodium nitrite (10.0 mmol in 1.50 mL of water) was added dropwise. The precipitate was filtered off and washed subsequently with water, ethanol, and diethyl ether before being dried in vacuo. Because of the low thermal stability, we solely performed ^{1}H NMR spectroscopy on the diazonium salts and used them in the following step immediately after preparation.

General Synthetic Procedure B. Synthesis of 1-*N,N*-dimethylsulfamoyl-5-phenylazoimidazoles.[30] 1-*N,N*-Dimethylsulfamoylimidazole was dissolved under a nitrogen atmosphere in dry THF (6 mL per mmol) and cooled to −78 °C. Then, *n*-BuLi (2.5 M in hexane, 1.0 equiv) was added slowly over 15 min, and the solution was stirred at −78 °C for 30 min. Dimethylthexylchlorosilane (1.0 equiv) was added; the cooling bath was removed, and stirring was continued at room temperature overnight. The solution was again cooled to −78 °C; *n*-BuLi (2.5 M in hexane, 1.1 equiv) was added slowly over 10 min, and the mixture was stirred at −78 °C for 30 min. Then, diazonium tetrafluoroborate (1.0 equiv) was added, and the reaction mixture immediately turned from light yellow to deep red. The cooling bath was removed, and the mixture was stirred at room temperature overnight. The reaction mixture was quenched with diluted aq $NaHCO_3$, layers were separated, and the aqueous layer was extracted once with THF. The combined organic layers were treated with TBAF trihydrate (1.5 equiv) and a spatula tip of cesium fluoride and were stirred at room temperature overnight. Diluted aq NaHCO3 was added; layers were separated, and the aqueous layer was extracted with DCM (3×). The combined organic layers were dried over $MgSO_4$ and evaporated. Purification was achieved via column chromatography on silica gel.

General Synthetic Procedure C. Synthesis of 1-trityl-4-phenylazoimidazoles.[30] The sulfamoyl-protected azo-imidazole was dissolved in EtOH/HCl (4:1) (25 mL/mmol), and the mixture was stirred at 50 °C for 3 h. After cooling to 0 °C (ice bath), the mixture was basified with 40% KOH (aq) (pH ∼10). The solution was extracted with $CHCl_3$ (3 × 25 mL); the combined organic layers were dried over $MgSO_4$ and evaporated to dryness. The residue was taken up in DCM (15 mL/mmol), treated with trityl chloride (1.1 equiv) and triethylamine (1.3 equiv), and stirred at room temperature overnight. The organic layer was washed with aq $NaHCO_3$ (2×), and the combined aq layers were extracted with DCM (2×). The combined organic layers were dried over $MgSO_4$, and the solvent was removed. Purification was achieved via column chromatography on silica gel.

General Synthetic Procedure D. Synthesis of 1-methyl-5-phenylazoimidazoles.[30] 1-Trityl-5-phenyl-azoimidazole was dissolved under nitrogen atmosphere in dry DCM (7.5 mL/mmol), and methyl triflate (1.2 equiv) was added via a syringe at room temperature. The reaction mixture was stirred at room temperature overnight; acetone/water (1:1, 15 mL/mmol) was added, and stirring was continued for an additional 4 h. Then, saturated $NaHCO_3$ was added, and the layers were separated. The aq layer was extracted with DCM (3×); the combined organic layers were dried over $MgSO_4$, and the solvent was removed. Purification was achieved via column chromatography on silica gel.

Synthesis of 1-Methyl-5-(phenylazo)imidazole (2). 1-Methyl-5-(phenylazo)imidazole (**2**) was synthesized and characterized as previously reported.[30]

*Synthesis of 1-Methyl-5-(4′-fluorophenylazo)imidazole (**2a**).* Step 1: 4-Fluorodiazoniumbenzene tetrafluoroborate. 4-Fluoroaniline (4.30 g, 45.0 mmol) was converted to the desired diazonium compound following general procedure A. The product was obtained as a white solid (7.31, 34.8 mmol, 77%). ^{1}H NMR (200 MHz, 300 K, CD_3CN): δ 8.72−8.50 (m, 2 H, 2,6-H), 7.78−7.55 (m, 2 H, 3,5-H) ppm. Step 2: 1-Dimethylsulfamoyl-5-(4′-fluorophenylazo)imidazole. Starting from 1-*N,N*-dimethyl-sulfamoylimidazole (2.00 g, 11.4 mmol), general procedure B was applied. Purification via column chromatography on silica gel (CH_2Cl_2/EtOAc (9:1), R_f = 0.51) gave the desired product as an orange-yellow solid (2.01 g, 6.75 mmol, 59%). Mp: 98 °C. FT-IR (layer) ν: 3142 (w), 2931 (w), 1592 (m), 1518 (w), 1501 (m), 1457 (m), 1388 (m), 1336 (m), 1226 (m), 1168 (s), 1143 (m), 1115 (m), 1091 (s), 1055 (m), 969 (s), 850 (s), 820 (s), 748 (m), 723 (s), 649 (m), 629 (m), 584 (s), 518 (s) cm^{-1}. ^{1}H NMR (500 MHz, 300 K, $CDCl_3$, TMS): δ 8.13 (s, 1 H, 2-H), 7.88−7.83 (m, 2 H, 2′,6′-H), 7.50 (s, 1 H, 4-H), 7.22−7.17 (m, 2 H, 3′,5′-H), 2.97 (s, 6 H, -N(CH_3)$_2$) ppm. ^{13}C NMR (125 MHz, 300 K, $CDCl_3$, TMS): δ 164.8 (C-4′), 149.6 (C-1′), 145.1 (C-5), 141.1 (C-2), 125.2 (C-2′,6′), 119.0 (C-4), 116.6 (C-3′,5′), 38.5 (-N(CH_3)$_2$) ppm. ^{19}F-NMR (470 MHz, 300 K, $CDCl_3$): δ −107.52 (s, 4′-F) ppm. MS (EI, 70 eV) *m*/*z* (%): 297 (42) $[M]^+$, 190 (44) $[M - DMS]^+$, 134 (100), 108 (40) $[SO_2NMe_2]^+$. MS (CI, isobutane) *m*/*z* (%): 298 (100) $[M + H]^+$, 123 (11). UV−vis (toluene) λ_{max} (lg ε): 357 nm (4.214). Anal. Calcd for $C_{11}H_{12}N_5O_2FS$: C, 44.44; H, 4.07; N, 23.56; S, 10.79. Found: C, 44.79; H, 4.04; N, 23.42; S, 10.71. Step 3: 1-Trityl-4-(4′-fluorophenylazo)imidazole. Starting from 1-dimethylsulfamoyl-5-(4′-fluoro-phenylazo)imidazole (1.00 g, 3.36 mmol), general procedure C was applied. Purification via column chromatography on silica gel (CH_2Cl_2/EtOAc (1:1), R_f = 0.80) gave the desired product as a yellow solid (884 mg, 2.04 mmol, 61%). Mp: 234 °C. FT-IR (layer) ν: 3059 (w), 1593 (m), 1492 (m), 1444 (m), 1322 (w), 1299 (m), 1222 (m), 1124 (m), 1090 (w), 1038 (w), 1001 (w), 846 (m), 749 (s), 702 (s), 658 (s), 639 (m), 528 (s) cm^{-1}. ^{1}H NMR (500 MHz, 300 K, $CDCl_3$, TMS): δ 7.92−7.88 (m, 2 H, 2′,6′-H), 7.54 (s, 1 H, 5-H), 7.52 (s, 1 H, 2-H), 7.39−7.36 (m, 9 H, *m*-Tr-H, *p*-Tr-H), 7.22−7.18 (m, 6 H, *o*-Tr-H), 7.16−7.10 (m, 2 H, 3′,5′-H) ppm. ^{13}C NMR (125 MHz, 300 K, $CDCl_3$, TMS): δ 164.1 (C-4′), 153.2 (C-4), 149.7 (C-1′), 141.9 (-CPh_3), 139.5 (C-2), 129.9 (C-*o*-Tr), 128.6 (C-*m*-Tr), 128.5 (C-*p*-Tr), 124.7 (C-

DOI: 10.1021/acs.joc.5b02817
J. Org. Chem. 2016, 81, 1206−1215

2′,6′), 122.5 (C-5), 116.0 (C-3′,5′) 76.4 (C-*i*-Tr) ppm. ^{19}F-NMR (470 MHz, 300 K, $CDCl_3$): δ −110.40 (s, 4′-F) ppm. MS (EI, 70 eV) *m*/*z* (%): 432 (1) $[M]^+$, 243 (100) $[Tr]^+$, 165 (42) $[Tr\text{-}Ph]^+$. MS (CI, isobutane) *m*/*z* (%): 433 (1) $[M + H]^+$, 243 (100) $[Tr]^+$, 191 (20) $[M - Tr + H]^+$, 167 (31) $[Tr - Ph + 2H]^+$. UV−vis (toluene) λ_{max} (lg ε): 336 nm (4.246). Anal. Calcd for $C_{28}H_{21}N_4F$: C, 77.76; H, 4.89; N, 12.95. Found: C, 77.80; H, 5.21; N, 12.96. Step 4: 1-Methyl-5-(4′-fluorophenylazo)imidazole (**2a**). Starting from 1-trityl-4-(4′-fluorophenylazo)-imidazole (400 mg, 925 μmol), general procedure D was applied. Purification via column chromatography on silica gel (EtOAc, R_f = 0.30) gave the desired product **2a** as a yellow solid (150 mg, 735 μmol, 79%). Mp: 113 °C. FT-IR (layer) ν: 3089 (w), 1588 (m), 1496 (m), 1429 (m), 1402 (w), 1345 (m), 1284 (m), 1232 (s), 1207 (s), 1170 (m), 1119 (s), 1096 (m), 1034 (m), 894 (w), 842 (s), 750 (m), 717 (m), 682 (m), 663 (s), 646 (s), 552 (m), 514 (s) cm^{-1}. ^{1}H NMR (500 MHz, 300 K, $CDCl_3$, TMS): δ 7.87−7.80 (m, 2 H, 2′,6′-H), 7.69 (s, 1 H, 2-H), 7.57 (s, 1 H, 4-H), 7.20−7.12 (m, 2 H, 3′,5′-H), 3.96 (s, 3 H, N-CH_3) ppm. ^{13}C NMR (125 MHz, 300 K, $CDCl_3$, TMS): δ 164.3 (C-4′), 149.7 (C-1′), 145.2 (C-5), 140.4 (C-2), 124.4 (C-2′,6′), 122.8 (C-4), 116.2 (C-3′,5′), 32.7 (N-CH_3) ppm. ^{19}F-NMR (470 MHz, 300 K, $CDCl_3$): δ −109.48 (s, br, 4′-F) ppm. MS (EI, 70 eV) *m*/*z* (%): 204 (100) $[M]^+$, 124 (15), 109 (39). MS (CI, isobutane) *m*/*z* (%): 205 (100) $[M + H]^+$. HR-MS (EI, 70 eV): *m*/*z* $[M]^+$ calcd for $C_{10}H_9N_4F$, 204.0811; found 204.0811. UV−vis (toluene) λ_{max} (lg ε): 362 nm (4.230).

*Synthesis of 1-Methyl-5-(4′-methoxyphenylazo)imidazole (**2b**).* Step 1: 4-Methoxydiazoniumbenzene tetrafluoroborate. 4-Anisidine (5.00 g, 40.6 mmol) was converted to the desired diazonium compound following general procedure A. The product was obtained as light purple solid (6.70, 30.2 mmol, 74%). ^{1}H NMR (200 MHz, 300 K, CD_3CN): δ 8.43 (s, 2 H, 2,6-H), 7.36 (s, 2 H, 3,5-H), 4.06 (s, 3 H, -OCH_3) ppm. Step 2: 1-Dimethylsulfamoyl-5-(4′-methoxyphenylazo)imidazole. Starting from 1-*N*,*N*-dimethyl-sulfamoylimidazole (2.00 g, 11.4 mmol), general procedure B was applied. Purification via column chromatography on silica gel (CH_2Cl_2/EtOAc (9:1), R_f = 0.49) gave the desired product as an orange-red solid (2.35 g, 7.60 mmol, 67%). Mp: 125 °C. FT-IR (layer) ν: 3134 (w), 2943 (w), 2838 (w), 1602 (m), 1582 (m), 1419 (m), 1454 (m), 1385 (s), 1251 (s), 1166 (s), 1138 (s), 1090 (s), 1023 (s), 972 (s), 890 (m), 841 (m), 808 (m), 723 (s), 651 (m), 634 (m), 584 (s), 551 (s), 529 (s) cm^{-1}. ^{1}H NMR (500 MHz, 300 K, $CDCl_3$, TMS): δ 8.09 (d, ^4J = 0.8 Hz, 1 H, 2-H), 7.85−7.82 (m, 2 H, 2′,6′-H), 7.45 (d, ^4J = 0.8 Hz, 1 H, 4-H), 7.02−6.98 (m, 2 H, 3′,5′-H), 3.90 (s, 3 H, -OCH_3), 2.97 (s, 6 H, -N(CH_3)$_2$) ppm. ^{13}C NMR (125 MHz, 300 K, $CDCl_3$, TMS): δ 162.7 (C-4′), 147.3 (C-1′), 145.1 (C-5), 140.3 (C-2), 125.0 (C-2′,6′), 118.1 (C-4), 114.5 (C-3′,5′), 55.7 (-OCH_3), 38.4 (-N(CH_3)$_2$) ppm. MS (EI, 70 eV) *m*/*z* (%): 309 (72) $[M]^+$, 202 (27) $[M - DMS + H]^+$. MS (CI, isobutane) *m*/*z* (%): 310 (100) $[M + H]^+$. UV−vis (toluene) λ_{max} (lg ε): 371 nm (4.314). Step 3: 1-Trityl-4-(4′-methoxyphenylazo)imidazole. Starting from 1-dimethylsulfamoyl-5-(4′-meth-oxyphenylazo)imidazole (1.00 g, 3.23 mmol), general procedure C was applied. Purification via column chromatography on silica gel (EtOAc, R_f = 0.74) gave the desired product as a yellow solid (1.30 g, 2.92 mmol, 90%). Mp: 190 °C. FT-IR (layer) ν: 3057 (w), 2838 (w), 1597 (m), 1578 (m), 1491 (m), 1442 (m), 1298 (w), 1244 (s), 1184 (m), 1143 (m), 1119 (m), 1029 (m), 991 (m), 839 (s), 808 (m), 747 (s), 700 (s), 655 (s), 536 (m) cm^{-1}. ^{1}H NMR (500 MHz, 300 K, $CDCl_3$, TMS): δ 7.91−7.86 (m, 2 H, 2′,6′-H), 7.50 (d, ^4J = 1.4 Hz, 1 H, 5-H), 7.49 (d, ^4J = 1.3 Hz, 1 H, 2-H), 7.39−7.36 (m, 9 H, *m*-Tr-H, *p*-Tr-H), 7.22−7.18 (m, 6 H, *o*-Tr-H), 6.98−6.94 (m, 2 H, 3′,5′-H), 3.86 (s, 3 H, -OCH_3) ppm. ^{13}C NMR (125 MHz, 300 K, $CDCl_3$, TMS): δ 161.5 (C-1′), 153.4 (C-4), 147.4 (C-3′,5′), 141.9 (C-*i*-Tr), 139.1 (C-2), 129.8 (C-*o*-Tr), 128.3 (C- *p*-Tr), 128.3 (C-*m*-Tr), 124.4 (C-2′,6′), 121.0 (C-5), 114.1 (C-3′,5′), 76.1 (-CPh$_3$), 55.5 (-OCH_3) ppm. MS (EI, 70 eV) *m*/*z* (%): 444 (1) $[M]^+$, 243 (100) $[Tr]^+$, 202 (15) $[M - Tr + H]^+$, 165 (42) $[Tr - Ph]^+$. MS (CI, isobutane) *m*/*z* (%): 445 (1) $[M + H]^+$, 243 (100) $[Tr]^+$, 203 (20) $[M - Tr + 2H]^+$. UV−vis (toluene) λ_{max} (lg ε): 360 nm (4.349). Anal. Calcd for $C_{29}H_{24}N_4O$: C, 78.36; H, 5.44; N, 12.60. Found: C, 78.15; H, 5.77; N, 12.36. Step 4: 1-Methyl-5-(4′-methoxyphenylazo)imidazole (**2b**). Starting from 1-trityl-4-(4′-methoxyphenyl-azo)imidazole (400 mg, 900 μmol), general procedure D was applied. Purification via column chromatography on silica gel (EtOAc, R_f = 0.32) gave desired product **2b** as an orange-yellow solid (179 mg, 828 μmol, 92%). Mp: 103 °C. FT-IR (layer) ν: 2916 (w), 1599 (m), 1581 (m), 1525 (w), 1495 (m), 1444 (m), 1343 (m), 1240 (s), 1143 (s), 1107 (m), 909 (m), 844 (s), 812 (s), 758 (m), 699 (m), 640 (s), 559 (s), 524 (s) cm^{-1}. ^{1}H NMR (500 MHz, 300 K, $CDCl_3$, TMS): δ 7.85−7.80 (m, 2 H, 2′,6′-H), 7.77 (s, 1 H, 2-H), 7.52 (s, 1 H, 4-H), 7.01−6.97 (m, 2 H, 3′,5′-H), 3.98 (s, 3 H, N-C H_3), 3.89 (s, 3 H, -OCH_3) ppm. ^{13}C NMR (125 MHz, 300 K, $CDCl_3$, TMS): δ 162.2 (C-1′), 147.5 (C-4′), 145.4 (C-5), 139.5 (C-2), 124.5 (C-2′,6′), 120.5 (C-4), 114.5 (C-3′,5′), 55.8 (-OCH_3), 32.6 (N-CH_3) ppm. MS (EI, 70 eV) *m*/*z* (%): 216 (100) $[M]^+$, 122 (15), 109 (16), 107 (60) $[C_7H_7O]^+$. MS (CI, isobutane) *m*/*z* (%): 217 (100) $[M + H]^+$. HR-MS (EI, 70 eV): *m*/*z* $[M]^+$ calcd for $C_{11}H_{12}N_4O$, 216.1011; found, 216.1020. UV−vis (toluene) λ_{max} (lg ε): 372 nm (4.284).

*Synthesis of 1-Methyl-5-(4′-N,N-dimethylaminophenylazo)-imidazole (**2c**).* Step 1: 4-*N*,*N*-Dimethylaminodiazoniumbenzene tetrafluoroborate. 4-*N*,*N*-Dimethylaminoaniline (3.70 g, 27.2 mmol) was converted into the desired diazonium compound following general procedure A. The product was obtained as a white solid (3.26 g, 13.9 mmol, 51%). ^{1}H NMR (200 MHz, 300 K, CD_3CN): δ 8.08−7.94 (m, 2 H, 2,6-H), 7.00−6.89 (m, 2 H, 3,5-H), 3.27 (s, 6 H, -N(CH_3)$_2$) ppm. Step 2: 1-Dimethylsulfamoyl-5-(4′-*N*,*N*-dimethylaminophenylazo)-imidazole. Starting from 1-*N*,*N*-dimethylsulfamoylimidazole (1.50 g, 8.57 mmol), general procedure B was applied. Purification via column chromatography on silica gel (CH_2Cl_2/EtOAc (9:1), R_f = 0.34) gave the desired product as a red solid (1.30 g, 4.03 mmol, 47%). Mp: 157 °C. FT-IR (layer) ν: 3116 (w), 2901 (w), 1598 (m), 1514 (m), 1460 (w), 1432 (m), 1417 (m), 1388 (m), 1353 (m), 1272 (m), 1231 (m), 1170 (m), 1087 (s), 959 (s), 886 (m), 844 (m), 823 (s), 725 (s), 702 (m), 631 (m), 594 (s), 524 (s) cm^{-1}. ^{1}H NMR (600 MHz, 300 K, $CDCl_3$, TMS): δ 8.04 (d, ^4J = 0.7 Hz, 1 H, 2-H), 7.80−7.77 (m, 2 H, 2′,6′-H), 7.36 (d, ^4J = 0.7 Hz, 1 H, 4-H), 6.75−6.71 (m, 2 H, 3′,5′-H), 3.11 (s, 6 H, C$^{4'}$-N(CH_3)$_2$), 2.96 (s, 6 H, -SO$_2$N(CH_3)$_2$) ppm. ^{13}C NMR (125 MHz, 300 K, $CDCl_3$, TMS): δ 152.8 (C-1′), 145.6 (C-5), 144.0 (C-4′), 139.2 (C-2), 125.4 (C-2′,6′), 116.9 (C-4), 111.6 (C-3′,5′), 40.3 (C$^{4'}$-N(CH_3)$_2$), 38.4 (-SO$_2$N(CH_3)$_2$) ppm. MS (EI, 70 eV) *m*/*z* (%): 322 (100) $[M]^+$, 214 (20) $[M\text{-}SO_2NMe_2]^+$. MS (CI, isobutane) *m*/*z* (%): 323 (100) $[M + H]^+$, 216 (13) $[M - SO_2NMe_2 + H]^+$. UV−vis (toluene) λ_{max} (lg ε): 455 nm (4.395). Anal. Calcd for $C_{13}H_{18}N_6O_2S$: C, 48.43; H, 5.63; N, 26.07; S, 9.95. Found: C, 48.85; H, 5.46; N, 25.79; S, 10.22. Step 3: 4(5)-(4′-*N*,*N*-Dimethylaminophenylazo)imidazole. 1-Dimethylsulfamoyl-5-(4′-*N*,*N*-dimethylaminophenylazo)imidazole (100 mg, 310 μmol) was dissolved in THF/HCl (4:1) (16 mL), and the mixture was heated to reflux for 1 h. The mixture was basified with 40% KOH (aq) (pH ∼10) and extracted with CH_2Cl_2 (3 × 50 mL). The combined organic layers were dried over $MgSO_4$ and evaporated to dryness. Purification via column chromatography on silica gel (EtOAc/acetone, 1:1) gave a red solid (33.0 mg, 153 μmol, 49%). ^{1}H NMR (500 MHz, 300 K, $CDCl_3$): δ 7.81−7.77 (m, 2 H, 2′,6′-H), 7.67 (d, ^4J = 0.8 Hz, 1 H, 5(4)-H), 7.64 (d, ^4J = 0.8 Hz, 1 H, 2-H), 6.75−6.71 (m, 2 H, 3′,5′-H), 3.06 (s, 6 H, -N(CH_3)$_2$) ppm. MS (EI, 70 eV) *m*/*z* (%): 215 (100) $[M]^+$, 149 (18) $[M - Im + H]^+$, 120 (19) $[C_8H_{10}N]^+$. MS (CI, isobutane) *m*/*z* (%): 216 (10) $[M + H]^+$. Step 4: 1-Trityl-4-(4′-*N*,*N*-dimethylaminophenylazo)-imidazole. 4(5)-(4′-*N*,*N*-Dimethylaminophenylazo)imidazole (186 mg, 767 μmol) was dissolved in CH_2Cl_2 (10 mL). The solution was treated with trityl chloride (235 mg, 844 μmol) and triethylamine (140 μL, 997 μmol) and stirred at room temperature overnight. The organic layer was washed twice with water, and the combined aq layers were extracted with DCM (2 × 20 mL). The combined organic layers were dried over $MgSO_4$, and the solvent was removed. Purification via column chromatography on silica gel (CH_2Cl_2/EtOAc (1:1), R_f = 0.67) gave the desired product as a yellow solid (230 mg, 503 μmol, 66%). Mp: 263 °C. FT-IR (layer) ν: 2906 (w), 1595 (s), 1511 (m), 1488 (m), 1442 (m), 1406 (w), 1361 (s), 1224 (m), 1147 (s), 1113 (m), 1035 (w), 986 (m), 942 (m), 865 (w), 823 (s), 751 (s), 704 (s), 655 (s), 526 (s) cm^{-1}. ^{1}H NMR (600 MHz, 300 K, $CDCl_3$, TMS): δ 7.86−7.84 (m, 2 H, 2′,6′-H), 7.46 (d, ^4J = 1.4 Hz, 1 H, 2-H), 7.41 (d, ^4J = 1.5 Hz, 1 H, 5-H), 7.37−7.34 (m, 9 H, *m*-Tr-H, *p*-Tr-H), 7.22−7.19 (m, 6 H, *o*-Tr-H), 6.73−6.70 (m, 2 H, 3′,5′-H), 3.03 (s, 6 H, -N(CH_3)$_2$) ppm. ^{13}C NMR (150 MHz, 300 K, $CDCl_3$, TMS): δ 153.6 (C-4), 152.0 (C-4′), 143.9 (C-1′), 142.0 (C-*i*-

DOI: 10.1021/acs.joc.5b02817
J. Org. Chem. 2016, 81, 1206−1215

Tr), 138.8 (C-2), 129.8 (C-*o*-Tr), 128.2 (C-*m*-Tr), 127.9 (C-*p*-Tr), 124.6 (C-2′,6′), 119.2 (C-5), 111.5 (C-3′,5′), 76.0 (-CPh_3), 40.3 (-$N(CH_3)_2$) ppm. MS (EI, 70 eV) *m*/*z* (%): 457 (5) $[M]^+$, 243 (100) $[Tr]^+$, 215 (10) $[M\text{-}Tr]^+$, 165 (41) $[Tr\text{-}Ph]^+$. MS (CI, isobutane) *m*/*z* (%): 458 (1) $[M + H]^+$, 243 (100) $[Tr]^+$, 216 (10) $[M - Tr + 2H]^+$, 167 (18) $[Tr - Ph + 2H]^+$. UV−vis (toluene) λ_{max} (lg ε): 402 nm (4.146). Step 5: 1-Methyl-5-(4′-*N*,*N*-dimethylaminophenylazo)imidazole (**2c**). Starting from 1-trityl-4-(4′-*N*,*N*-dimethylaminophenylazo)-imidazole (220 mg, 481 μmol), general procedure D was applied. Purification via column chromatography on silica gel (acetone, R_f = 0.52) gave desired product **2c** as a red solid (60.0 mg, 262 μmol, 54%). Mp: 126 °C. FT-IR (layer) ν: 3120 (w), 2917 (m), 2820 (w), 2652 (w), 1600 (s), 1557 (m), 1506 (m), 1445 (m), 1367 (s), 1311 (m), 1278 (m), 1231 (m), 1144 (s), 1108 (s), 1069 (s), 942 (m), 892 (m), 821 (s), 796 (s), 711 (m), 669 (s), 642 (s), 529 (s) cm^{-1}. ^1H NMR (500 MHz, 300 K, $CDCl_3$, TMS): δ 7.80−7.76 (m, 2 H, 2′,6′-H), 7.54 (s, 1 H, 2-H), 7.42 (d, ^4J = 0.9 Hz, 1 H, 4-H), 6.76−6.72 (m, 2 H, 3′,5′-H), 3.92 (s, 3 H, -CH_3), 3.08 (s, 6 H, $C^{4'}$-$N(CH_3)_2$) ppm. ^{13}C NMR (125 MHz, 300 K, $CDCl_3$, TMS): δ 152.3 (C-1′), 145.8 (C-5), 144.2 (C-4′), 139.0 (C-2), 124.5 (C-2′,6′), 120.1 (C-4), 111.7 (C-3′,5′), 40.5 ($C^{4'}$-$N(CH_3)_2$), 32.2 (−CH_3) ppm. MS (EI, 70 eV) *m*/*z* (%): 229 (100) $[M]^+$, 105 (10) $[C_6H_5N_2]^+$. MS (CI, isobutane) *m*/*z* (%): 230 (100) $[M + H]^+$. HR-MS (EI, 70 eV): *m*/*z* $[M]^+$ calcd for $C_{12}H_{15}N_5$, 229.1328; found, 229.1323. UV−vis (toluene) λ_{max} (lg ε): 440 nm (4.339).

*Synthesis of 1-Methyl-5-(3′,5′-di-tert-butyl-4′-methoxyphenylazo)imidazole (**2e**).* Step 1: 3,5-Di-*tert*-butyl-4-methoxybenzoic acid. 3,5-Di-*tert*-butyl-4-hydroxybenzoic acid (10.0 g, 39.9 mmol) was dissolved in acetone (200 mL) and treated with potassium hydroxide (5.60 g, 100 mmol) and iodomethane (7.40 mL, 120 mmol). The reaction mixture was heated to 60° and stirred under reflux for 18 h. The mixture was partially evaporated and treated with ethyl acetate and water. Layers were separated, and the aqueous layer was extracted three times with ethyl acetate. The combined organic layers were dried over magnesium sulfate and evaporated to dryness. The residue was dissolved in THF/water (1:1, 100 mL) and treated with lithium hydroxide monohydrate (5.00 g, 119 mmol). The reaction mixture was stirred at 60 °C for 18 h. The solution was partially evaporated and acidified with concd HCl. The precipitate was filtered off and recrystallized from CH_2Cl_2/*n*-hexane (1:1). The desired product was obtained as a colorless solid (7.49 g, 26.7 mmol, 71%). ^1H NMR (200 MHz, 300 K, $CDCl_3$, TMS): δ 8.04 (d, ^4J = 0.4 Hz, 2 H, 2-H), 3.74 (s, 3 H, -OCH_3), 1.47 (s, 18 H, 2x -$C(CH_3)_3$) ppm. Step 2: 3,5-Di-*tert*-butyl-4-methoxyphenylcarbamic *tert*-butylester. 3,5-Di-*tert*-butyl-4-methoxybenzoic acid (3.00 g, 11.4 mmol) was treated with triethylamine (1.66 mL, 11.4 mmol) and DPPA (2.60 mL, 11.4 mmol) in *tert*-butanol (50.0 mL). The mixture was stirred at 85 °C overnight, and after cooling, the precipitate was filtered off multiple times and washed with little EtOH to yield 3,5-di-*tert*-butyl-4-methoxyphenylcarbamic *tert*-butylester as a white solid (2.75 g, 8.2 mmol, 72%). ^1H NMR (500 MHz, 300 K, $CDCl_3$, TMS): δ 7.21 (s, 2 H, 2,6-H), 6.32 (br s, 1 H, NH), 3.66 (s, 3 H, -OCH_3), 1.51 (s, 9 H, -$OC(CH_3)_3$), 1.42 (s, 18 H, 2x Ar-$C(CH_3)_3$) ppm. ^{13}C NMR (125 MHz, 300 K, $CDCl_3$, TMS): δ 223.7 (-N-*C*O-O-), 155.3 (C-4), 144.1 (C-3,5), 123.9 (C-1), 117.5 (C-2,6), 80.0 (O-$C(CH_3)_3$), 64.2 (-OCH_3), 35.9 (2x Ar-$C(CH_3)_3$), 32.0 (2x Ar-$C(CH_3)_3$), 28.4 (O-$C(CH_3)_3$) ppm. MS (EI, 70 eV) *m*/*z* (%): 335 (17) $[M]^+$, 279 (100) $[M - {}^tBu + H]^+$, 220 (21) $[C_{15}H_{24}O]^+$. MS (CI, isobutane) *m*/*z* (%): 336 (18) $[M + H]^+$, 280 (100) $[M - {}^tBu + 2H]^+$. Step 3:3,5-Di-*tert*-butyl-4-methoxyaniline. 3,5-Di-*tert*-butyl-4-methoxyphenylcarbamic *tert*-butylester (335 mg, 10.0 mmol) was dissolved in DCM (6.0 mL) and treated with trifluoracetic acid (1.0 mL). After stirring overnight at room temperature, the mixture was treated with sodium hydroxide (1.00 g) in water (6.0 mL) and extracted with DCM (3 × 30 mL). The organic layer was separated and dried over magnesium sulfate, and the solvent was evaporated in vacuo to give 3,5-di-*tert*-butyl-4-methoxy-aniline as a white solid (217 mg, 923 μmol, 92%). ^1H NMR (200 MHz, 300 K, $CDCl_3$, TMS): δ 6.55 (s, 2 H, 2,6-H), 3.57 (s, 3 H, -OCH_3), 3.41 (s, br, 2 H, NH_2), 1.33 (s, 18 H, 2x -$C(CH_3)_3$) ppm. Step 4: 3,5-Di-*tert*-butyl-4-methoxydiazoniumbenzene tetrafluoroborate. 3,5-Di-*tert*-butyl-4-methoxyaniline (2.25 g, 9.57 mmol) was dissolved in EtOH (22.5 mL) and 50% HBF_4 (2.00 mL). Isopentyl nitrite (1.35 mL, 10.1 mmol) was added dropwise and stirred for 15 min at room temperature. Then, 50% HBF_4 (5.0 mL) and water (30.0 mL) were added. The precipitate was filtered off and washed with little EtOH. The desired product was obtained as a light purple solid (2.07 g, 9.57 mmol, 65%), which was rather unstable and therefore was immediately used after preparation. ^1H NMR (200 MHz, 300 K, CD_3CN): δ 8.48 (s, 2 H, 2,6-H), 3.47 (s, 3 H, -OCH_3), 1.53 (s, 18 H, 2x -$C(CH_3)_3$) ppm. Step 5: 1-Dimethylsulfamoyl-5-(3′,5′-di-*tert*-butyl-4′-methoxyphenylazo)-imidazole. Starting from 1-*N*,*N*-dimethylsulfamoylimidazole (1.00 g, 5.71 mmol), general procedure B was applied. Purification via column chromatography on silica gel (CH_2Cl_2/EtOAc (19:1), R_f = 0.43) gave the desired product as an orange-red solid (1.40 g, 3.32 mmol, 58%). Mp: 114 °C. FT-IR (layer) ν: 3142 (w), 2956 (m), 1455 (m), 1387 (s), 1223 (m), 1162 (s), 1093 (s), 1003 (m), 972 (m), 889 (w), 834 (w), 750 (w), 726 (s), 638 (m), 591 (s), 537 (m), 513 (s) cm^{-1}. ^1H NMR (500 MHz, 300 K, $CDCl_3$, TMS): δ 8.12 (s, 1 H, 2-H), 7.81 (s, 2 H, 2′,6′-H), 7.46 (s, 1 H, 4-H), 3.75 (s, 3 H, -OCH_3), 3.01 (s, 6 H, -$SO_2N(CH_3)_2$), 1.47 (s, 18 H, 2x -$C(CH_3)_3$) ppm. ^{13}C NMR (125 MHz, 300 K, $CDCl_3$, TMS): δ 163.3 (C-4′), 148.2 (C-1′), 145.2 (C-3′,5′), 145.1 (C-5), 140.3 (C-2), 121.9 (C-2′,6′), 117.8 (C-4), 64.5 (-OCH_3), 38.4 (-$SO_2N(CH_3)_2$), 36.0 (2x -$C(CH_3)_3$), 31.9 (2x -$C(CH_3)_3$) ppm. MS (EI, 70 eV) *m*/*z* (%): 421 (100) $[M]^+$, 314 (30) $[M - SO_2NMe_2 + H]^+$, 257 (35) $[M - SO_2NMe_2 - {}^tBu + H]^+$, 234 (10). MS (CI, isobutane) *m*/*z* (%): 422 (100) $[M + H]^+$. UV−vis (toluene) λ_{max} (lg ε): 368 nm (4.204). Step 6: 1-Trityl-4-(3′,5′-di-*tert*-butyl-4′-methoxyphenylazo)imidazole. Starting from 1-dimethyl-sulfamoyl-5-(3′,5′-di-*tert*-butyl-4′-methoxyphenylazo)imidazole (1.10 g, 2.61 mmol), general procedure C was applied. Purification via column chromatography on silica gel ($CHCl_3$, R_f = 0.75) gave the desired product as an orange-yellow solid (1.12 g, 2.01 mmol, 77%). Mp: 208 °C. FT-IR (layer) ν: 2956 (w), 1491 (w), 1444 (m), 1407 (w), 1282 (w), 1218 (m), 1157 (w), 1119 (m), 1009 (m), 893 (w), 859 (w), 754 (s), 700 (s), 660 (m), 639 (m), 504 (m) cm^{-1}. ^1H NMR (500 MHz, 300 K, $CDCl_3$, TMS): δ 7.85 (s, 2 H, 2′,6′-H), 7.80 (d, ^4J = 1.6 Hz, 1 H, 5-H), 7.52 (d, ^4J = 1.4 Hz, 1 H, 2-H), 7.42−7.38 (m, 9 H, *m*-Tr-H, *p*-Tr-H), 7.21−7.17 (m, 6 H, *o*-Tr-H), 3.72 (s, 3 H, -OCH_3), 1.44 (s, 18 H, 2x -$C(CH_3)_3$) ppm. ^{13}C NMR (125 MHz, 300 K, $CDCl_3$, TMS): δ 162.1 (C-4′), 153.3 (C-4), 148.4 (C-1′), 144.5 (C-3′,5′), 142.0 (C-*i*-Tr), 139.0 (C-2), 129.9 (C-*o*-Tr), 128.4 (C-*m*-Tr), 128.0 (C-*p*-Tr), 121.6 (C-2′,6′), 121.3 (C-5), 76.3 (-CPh_3), 64.5 (-OCH_3), 36.2 (2x -$C(CH_3)_3$), 32.1 (2x -$C(CH_3)_3$) ppm. MS (EI, 70 eV) *m*/*z* (%): 260 (34), 243 (100) $[Tr]^+$, 183 (100), 165 (31) $[Tr\text{-}Ph]^+$, 105 (92). MS (CI, isobutane) *m*/*z* (%): 557 (4) $[M + H]^+$, 315 (14) $[M - Tr + H]^+$, 243 (100) $[Tr]^+$, 236 (17). UV−vis (toluene) λ_{max} (lg ε): 344 nm (4.152). Step 7: 1-Methyl-5-(3′,5′-di-*tert*-butyl-4′-methoxyphenylazo)imidazole (**2e**). Starting from 1-trityl-4-(3′,5′-di-*tert*-butyl-4′-methoxyphenylazo)imidazole (800 mg, 1.44 mmol), general procedure D was applied. Purification via column chromatography on silica gel (EtOAc, R_f = 0.55) gave desired product **2e** as an orange-yellow solid (388 mg, 1.18 mmol, 82%). Mp: 107 °C. FT-IR (layer) ν: 3102 (w), 2956 (m), 1503 (m), 1405 (m), 1340 (m), 1246 (w), 1219 (s), 1169 (m), 1114 (s), 996 (m), 893 (m), 809 (m), 643 (m), 597 (m), 535 (m) cm^{-1}. ^1H NMR (500 MHz, 300 K, toluene-d_8, toluene-d_8): δ 7.98 (s, 2 H, 2′,6′-H), 7.84 (s, br, 1 H, 4-H), 6.94 (s, br, 1 H, 2-H), 3.40 (s, 3 H, -OCH_3), 3.09 (s, 3 H, N-CH_3), 1.44 (s, 18 H, 2x -$C(CH_3)_3$) ppm. ^{13}C NMR (125 MHz, 300 K, toluene-d_8, toluene-d_8): δ 162.3 (C-4′), 149.3 (C-1′), 145.8 (C-5), 144.8 (C-3′,5′), 140.5 (C-2), 124.0 (C-4), 121.5 (C-2′,6′), 64.3 (-OCH_3), 36.2 (2x -$C(CH_3)_3$), 32.1 (2x -$C(CH_3)_3$), 31.4 (N-CH_3) ppm. MS (EI, 70 eV) *m*/*z* (%): 328 (74) $[M]^+$. MS (CI, isobutane) *m*/*z* (%): 329 (33) $[M + H]^+$. HR-MS (EI, 70 eV): *m*/*z* $[M]^+$ calcd for $C_{19}H_{28}N_4O$, 328.2263; found, 328.2261. UV−vis (toluene) λ_{max} (lg ε): 369 nm (4.156). Anal. Calcd for $C_{19}H_{28}N_4O$: C, 69.48; H, 8.59; N, 17.06. Found: C, 69.38; H, 8.61; N, 16.88.

■ ASSOCIATED CONTENT

Supporting Information

The Supporting Information is available free of charge on the ACS Publications website at DOI: 10.1021/acs.joc.5b02817.

Details of computational studies, ^1H NMR, ^{13}C NMR, and UV−vis spectra for compounds **2a−c** and **2e**, details of ^1H

DOI: 10.1021/acs.joc.5b02817
J. Org. Chem. 2016, 81, 1206−1215

NMR titration experiments, and details of ^{1}H NMR LD-CISSS experiments (PDF)

AUTHOR INFORMATION

Corresponding Author

*E-mail: rherges@oc.uni-kiel.de.

Notes

The authors declare no competing financial interest.

ACKNOWLEDGMENTS

We gratefully acknowledge financial support by the Deutsche Forschungsgemeinschaft via the collaborative research center SFB 677 "Function by Switching".

REFERENCES

(1) Szymanski, W.; Beierle, J. M.; Kistemaker, H. A. V.; Velema, W. A.; Feringa, B. L. *Chem. Rev.* **2013**, *113*, 6114−6178.

(2) Hilf, R. J. C.; Bertozzi, C.; Zimmermann, I.; Reiter, A.; Trauner, D.; Dutzler, R. *Nat. Struct. Mol. Biol.* **2010**, *17*, 1330−1336.

(3) Polosukhina, A.; Litt, J.; Tochitsky, I.; Nemargut, J.; Sychev, Y.; De Kouchkovsky, I.; Huang, T.; Borges, K.; Trauner, D.; Van Gelder, R.; Kramer, R. *Neuron* **2012**, *75*, 271−282.

(4) Kahn, O. *Molecular Magnetism*; VCH, 1993; p 380.

(5) Decurtins, S.; Gütlich, P.; Köhler, C. P.; Spiering, H.; Hauser, A. *Chem. Phys. Lett.* **1984**, *105*, 1−4.

(6) Gütlich, P.; Garcia, Y.; Goodwin, H. A. *Chem. Soc. Rev.* **2000**, *29*, 419−427.

(7) Gütlich, P.; Goodwin, H. A. *Spin Crossover in Transition Metal Compounds I*; Springer, 2004.

(8) Gopakumar, T. G.; Matino, F.; Naggert, H.; Bannwarth, A.; Tuczek, F.; Berndt, R. *Angew. Chem.* **2012**, *124*, 6367−6371.

(9) Gopakumar, T. G.; Matino, F.; Naggert, H.; Bannwarth, A.; Tuczek, F.; Berndt, R. *Angew. Chem., Int. Ed.* **2012**, *51*, 6262−6266.

(10) Thies, S.; Sell, H.; Schütt, C.; Bornholdt, C.; Näther, C.; Tuczek, F.; Herges, R. *J. Am. Chem. Soc.* **2011**, *133*, 16243−16250.

(11) Venkataramani, S.; Jana, U.; Dommaschk, M.; Sönnichsen, F. D.; Tuczek, F.; Herges, R. *Science* **2011**, *331*, 445−448.

(12) Thies, S.; Sell, H.; Bornholdt, C.; Schütt, C.; Köhler, F.; Tuczek, F.; Herges, R. *Chem. - Eur. J.* **2012**, *18*, 16358−16368.

(13) Dommaschk, M.; Schütt, C.; Venkataramani, S.; Jana, U.; Näther, C.; Sönnichsen, F. D.; Herges, R. *Dalton Trans.* **2014**, *43*, 17395−17405.

(14) Caughey, W. S.; Deal, R. M.; McLees, B. D.; Alben, J. O. *J. Am. Chem. Soc.* **1962**, *84*, 1735−1736.

(15) Caughey, W. S.; Fujimoto, W. Y.; Johnson, B. P. *Biochemistry* **1966**, *5*, 3830−3843.

(16) McLees, B. D.; Caughey, W. S. *Biochemistry* **1968**, *7*, 642−652.

(17) Cole, S. J.; Curthoys, G. C.; Magnusson, E. A.; Phillips, J. N. *Inorg. Chem.* **1972**, *11*, 1024−1028.

(18) Kim, D.; Su, Y. O.; Spiro, T. G. *Inorg. Chem.* **1986**, *25*, 3988−3993.

(19) Song, Y.; Haddad, R. E.; Jia, S.-L.; Hok, S.; Olmstead, M. M.; Nurco, D. J.; Schore, N. E.; Zhang, J.; Ma, J.-G.; Smith, K. M.; Gazeau, S.; Pécaut, J.; Marchon, J.-C.; Medforth, C. J.; Shelnutt, J. A. *J. Am. Chem. Soc.* **2005**, *127*, 1179−1192.

(20) Thies, S.; Bornholdt, C.; Köhler, F.; Sönnichsen, F. D.; Näther, C.; Tuczek, F.; Herges, R. *Chem. - Eur. J.* **2010**, *16*, 10074−10083.

(21) Dommaschk, M.; Peters, M.; Gutzeit, F.; Schütt, C.; Näther, C.; Sönnichsen, F. D.; Tiwari, S.; Riedel, C.; Boretius, S.; Herges, R. *J. Am. Chem. Soc.* **2015**, *137*, 7552−7555.

(22) Otsuki, J.; Narutaki, K. *Bull. Chem. Soc. Jpn.* **2004**, *77*, 1537−1544.

(23) Otsuki, J.; Narutaki, K.; Bakke, J. M. *Chem. Lett.* **2004**, *33*, 356−357.

(24) Suwa, K.; Otsuki, J.; Goto, K. *Tetrahedron Lett.* **2009**, *50*, 2106−2108.

(25) Suwa, K.; Otsuki, J.; Goto, K. *J. Phys. Chem. A* **2010**, *114*, 884−890.

(26) Weston, C. E.; Richardson, R. D.; Haycock, P. R.; White, A. J. P.; Fuchter, M. J. *J. Am. Chem. Soc.* **2014**, *136*, 11878−11881.

(27) Tabata, M.; Nishimoto, J. Equilibrium data of porphyrins and metalloporphyrins. *Porphyrin Handb.* **2000**, 221−419.

(28) Walker, F. A.; Lo, M.-W.; Ree, M. T. *J. Am. Chem. Soc.* **1976**, *98*, 5552−5560.

(29) Portela, C. F.; Magde, D.; Traylor, T. G. *Inorg. Chem.* **1993**, *32*, 1313−1320.

(30) Wendler, T.; Schütt, C.; Näther, C.; Herges, R. *J. Org. Chem.* **2012**, *77*, 3284−3287.

(31) *TURBOMOLE*, V6.3, 2011; a development of University of Karlsruhe and Forschungszentrum Karlsruhe GmbH, 1989−2007, TURBOMOLE GmbH, since 2007; available from http://www.turbomole.com.

(32) Herges, R.; Jansen, O.; Tuczek, F.; Venkatamarani, S. Photosensitive metal porphyrin complexes with pendant photoisomerizable chelate arm as photochromic molecular switches undergoing photoinduced spin transition. Patent DE 102010034496 A1, Feb 16, 2012.

(33) Herges, R.; Jansen, O.; Tuczek, F.; Venkatamarani, S. Transition metal complexes with photosensitive tethered ligands as visible light-induced spin-crossover magnetic molecular switches. Patent WO 2012022299 A1, Feb 23, 2012.

(34) Dommaschk, M.; Gutzeit, F.; Boretius, S.; Haag, R.; Herges, R. *Chem. Commun.* **2014**, *50*, 12476−12478.

(35) Chadwick, D. J.; Ngochindo, R. I. *J. Chem. Soc., Perkin Trans. 1* **1984**, 481−486.

(36) Dunker, M. F. W.; Starkey, E. B.; Jenkins, G. L. *J. Am. Chem. Soc.* **1936**, *58*, 2308−2309.

DOI: 10.1021/acs.joc.5b02817
J. Org. Chem. 2016, 81, 1206−1215